

# Spatially resolved electrochemical sensing of chemical gradients

Meghan M. Mensack,<sup>a</sup> John B. Wydallis,<sup>a</sup> N. Scott Lynn Jr.,<sup>b</sup> David S. Dandy,<sup>c</sup> and Charles S. Henry<sup>a, c, \*</sup>

<sup>a</sup>Department of Chemistry, Colorado State University, Fort Collins, CO, 80523

<sup>b</sup>Institute of Photonics and Electronics, Academy of Sciences of the Czech Republic, Prague, Czech Republic

<sup>c</sup>Department of Chemical and Biological Engineering, Colorado State University, Fort Collins, CO, 80523

## Electronic Supplementary Information

### Design, Fabrication, and Operation of Device

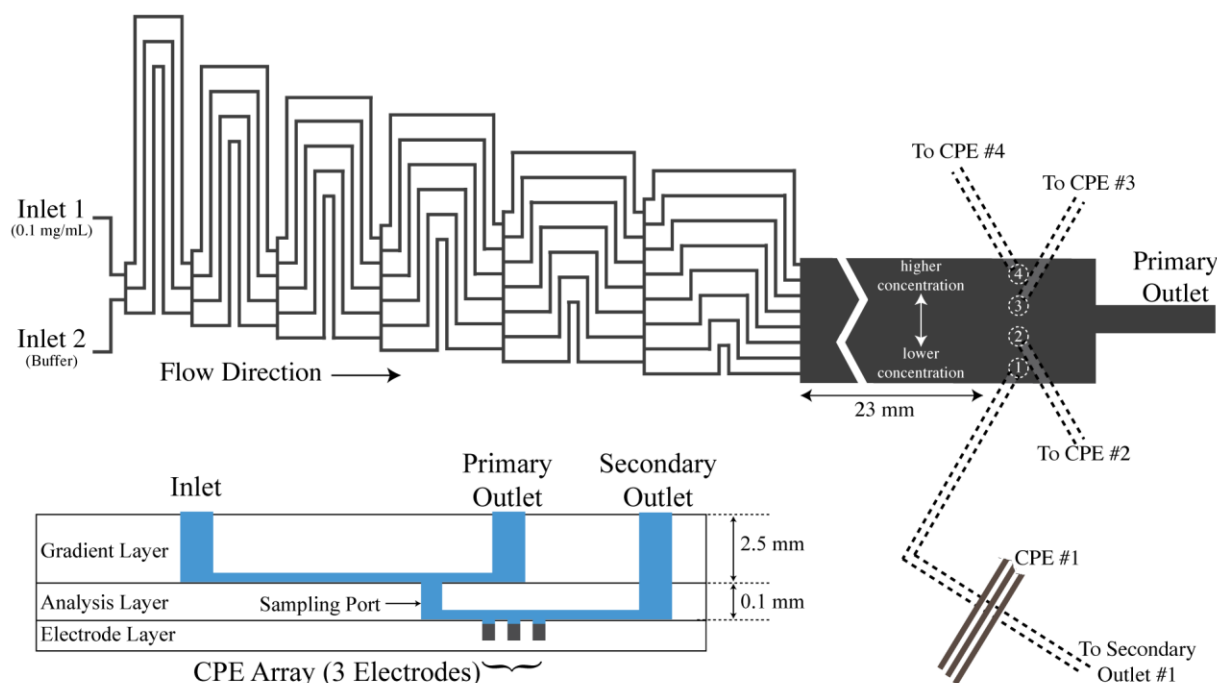


**Figure S1.** Design of the gradient generator overlaid with the vertical sample ports, numbered 1 to 4.

All three layers of the device are fabricated from poly(dimethyl) siloxane (PDMS) using standard soft lithography processes.<sup>1</sup> An expanded view of the three layers can be seen in Figure S1. The topmost (Gradient) layer consists of two inlets leading to a series of 50  $\mu\text{m}$  wide, 41  $\mu\text{m}$  tall microchannels set up in an expanding branched network. A stable spatial and temporal chemical gradient can be created in the main chamber by introducing either a fluorescent (fluorescein) or electrochemically active (dopamine) agent into one of the inlets. The flow within these channels is systematically split and recombined with each other in a fashion that leads to a monotonically decreasing concentration profile in the 8 outputs of the gradient generator. Details on this gradient generation method can be found in Jeon et al.<sup>2</sup> The 8 output channels of the gradient generator are introduced into a larger, 2 mm wide, 30 mm long, 41  $\mu\text{m}$  high main chamber that leads directly to the primary device outlet on the same layer. In the main chamber, a series of 4 (130  $\mu\text{m}$  diameter) vertical sample ports are situated 23 mm downstream from the output of the gradient generator, where the sampling ports are equally spaced in a line

orthogonal to the fluid flow direction. The sample ports lead to 4 individual analysis microchannels (100  $\mu\text{m}$  wide, 41  $\mu\text{m}$  high) fabricated into the bottom of the 2<sup>nd</sup> (Analysis) layer, each oriented orthogonal to a 3-electrode CPE array fabricated onto the top of the 3<sup>rd</sup> (Electrode) layer. Electrodes were fabricated using graphite, carbon nanotubes, and a binding agent using previously published methods.<sup>3</sup> Each analysis microchannel has an overall length of 18 mm, where the distance from the sample port to the electrode array is 7.5 mm. The layout of the fluidic portion of this device (Gradient and analysis layers) was designed such that for pressure driven flow of an aqueous fluid (Water at 20 °C has viscosity  $\eta = 0.001 \text{ g mm}^{-1} \text{ s}^{-1}$ ), 50% of the fluid will exit the device through the primary outlet, and 12.5% of the fluid will flow through each analysis microchannel and out of a secondary outlet. Because the design of the primary and secondary outlet microchannels are independent of one another, these flow ratios can be customized to values other than those used in this study.

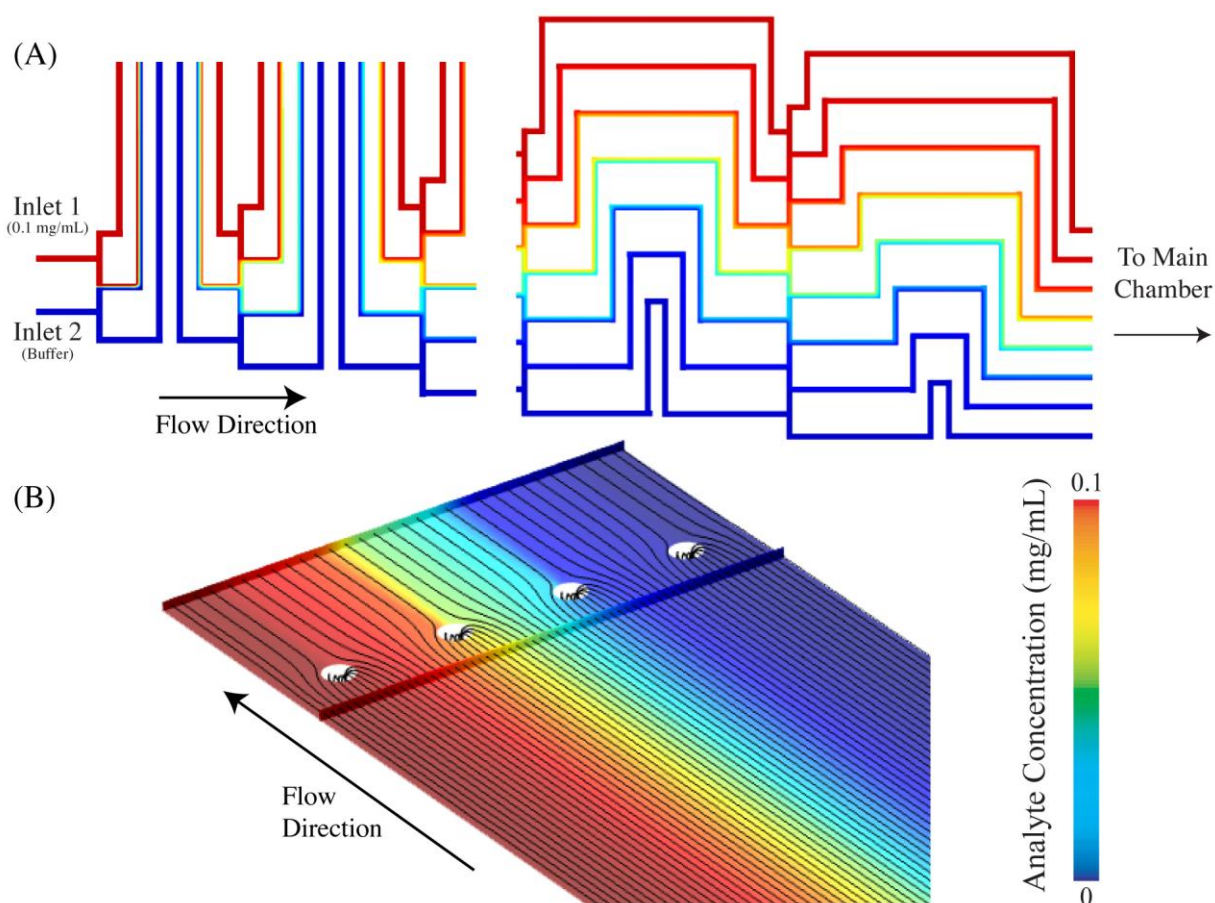
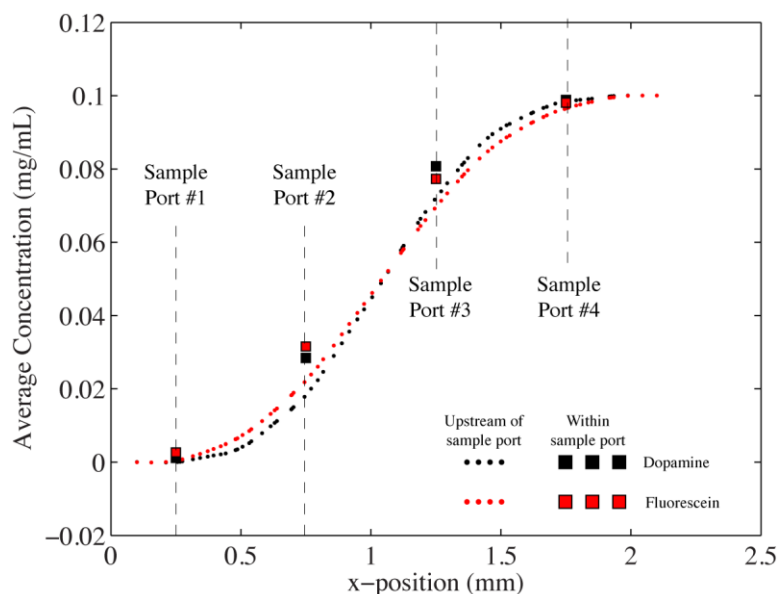


**Figure S2.** (A) COMSOL simulation of the convection and diffusion of fluorescein within the gradient generator. The flow rates of each inlet stream are 10  $\mu\text{L}/\text{min}$ , where one inlet has a concentration of 0.1 mg/mL of fluorescein. (B) Contours of fluorescein and flow streamlines near the sample ports.

### COMSOL Model – convection and diffusion profile

To ensure that the device is working correctly, we have employed the use of the finite element package COMSOL to simulate the transport of analyte through the topmost layer of the device. The flow rates of water through the microchannels shown in Figure S1 are well within the Stokes regime, and the fluid is void of any

turbulence. As a result, the convective and diffusive transport of analyte through the system can be modeled accurately via the solutions to both the Navier Stokes equations and the convection-diffusion equation. These simulations utilized a mesh with a characteristic size of 2.5 and 5 microns in the gradient generator and main chamber, which was predetermined such that the solution is independent of the mesh density. Typical 3D solutions consisted of over 300,000 hexahedral elements with 1.3 million degrees of freedom. The solution to the velocity, pressure, and concentration fields were obtained using the generalized minimal residual iterative solver, using a successive under-relaxation method for the pre- and post-smoother (with a PARDISO course solver). We employed a constant velocity condition on the two inlets, with the two inlets having an analyte concentration of 0 and 0.1 mg/mL, respectively. Because the simulation domain consisted of only the gradient layer, we employed a constant backpressure of  $p = 10$  Pa on each analysis port outlet (each outlet was extended 0.1 mm from the floor of the main chamber. This backpressure was chosen such that the volumetric flow rate exiting the primary outlet was 10  $\mu\text{L}/\text{min}$ , with 2.5  $\mu\text{L}/\text{min}$  flowing through each sample port. Solutions of this type were obtained for both fluorescein ( $D = 5 \times 10^{-6}$  cm/s) and dopamine ( $D = 2.7 \times 10^{-6}$  cm/s).



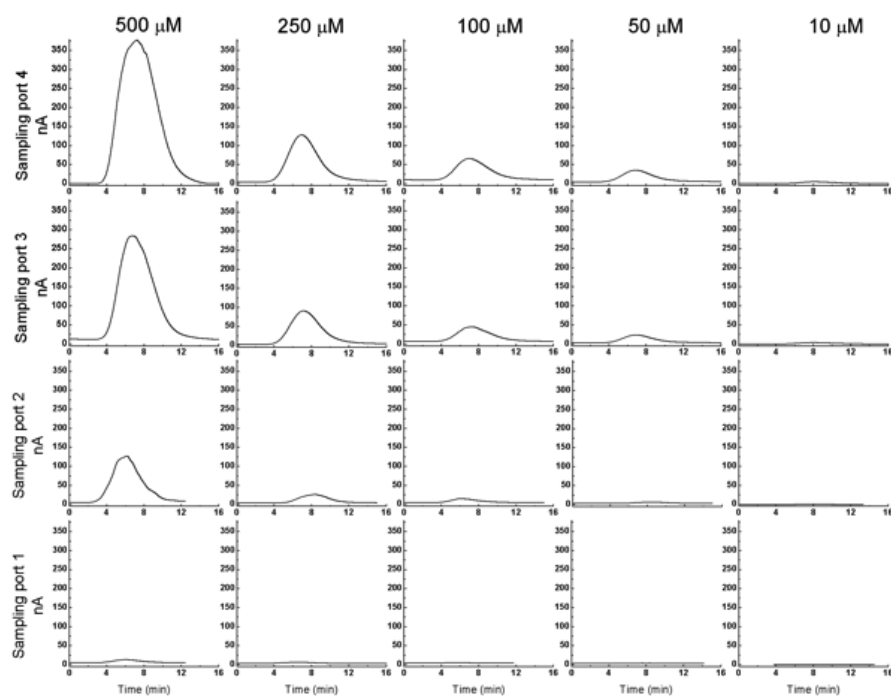
**Figure S3.** Average concentration of fluorescein and dopamine across the width of the main chamber (0.5 mm upstream of the sample ports). This data was taken from the results shown in Figure S2. The average concentration of both analytes entering each sample port is also shown.

Figure S2A displays contours of analyte through the first and last sections of the gradient generator. As expected, the concentration of analyte decreases monotonically from top to bottom. The average fluorescein concentration in the 8 outlet channels of the gradient generator (top to bottom) is 0.1, 0.096, 0.086, 0.068, 0.043, 0.020, 0.0057, and 0 mg/mL. Similarly, for dopamine these values are 0.26, 0.098, 0.09, 0.07, 0.041, 0.017, 0.003, and 0 mg/mL. The 8 channels of the gradient generator enter the main flow chamber where diffusion orthogonal to the flow direction acts to smooth the chemical gradient before reaching the sample ports. Figure S2B displays the contours of analyte (fluorescein) along the floor of the microchannel in the region of the sample ports. Fluid streamlines (shown in black) are positioned 10  $\mu\text{m}$  above the floor of the channel. It can be seen that the fluid near the channel floor will

be drawn into a sample port situated directly downstream of the region in question. Therefore the concentration in each analysis microchannel can be assumed to represent the concentration of analyte in the region just above each sample port.

From the results shown in Figure S2, we can calculate the average analyte concentration across the channel width situated 0.5 mm upstream of the sample ports. Figure S3 plots the average concentration of both fluorescein and dopamine across the channel width along with the average concentration of each analyte entering the 4 sample ports. These results parallel the experimental measurements for fluorescein (optical) and dopamine (electrochemical) seen in Figure 3. Figure Because each sample port is collecting fluid within a radius larger than the characteristic size of each sample port, as seen in the fluid streamlines in Figure S2, the average concentration in each port will be slightly higher than the concentration of analyte directly upstream of the center of each port. This effect can be resolved by decreasing the flow rate through each analysis channel, accomplished by increasing the viscous resistance of the network of analysis microchannels (e.g. lengthening each channel).

## Electrochemical results



**Figure S4.** Signal vs. time for the spatial and temporal electrochemical detection of dopamine.

## References

1. Y. N. Xia and G. M. Whitesides, *Angew Chem Int Edit*, 1998, **37**, 551-575.
2. N. L. Jeon, S. K. W. Dertinger, D. T. Chiu, I. S. Choi, A. D. Stroock and G. M. Whitesides, *Langmuir*, 2000, **16**, 8311-8316.
3. Y. Sameenoi, M. M. Mensack, K. Boonsong, R. Ewing, W. Dungchai, O. Chailapakul, D. M. Cropek and C. S. Henry, *Analyst*, 2011, **136**, 3177-3184.